Pergamon

Int. J. Heat Mass Transfer. Vol. 37, No. 4, pp. 571–579, 1994

0017-9310/94 $6.00+0.00

Modeling liquid-side particulate fouling in enhanced tubes

L. M. CHAMRA and R. L. WEBB

Department of Mechanical Engineering, The Pennsylvania State University, University Park, PA 16802, U.S.A.

(*Received* 3 *March* 1993 *and in final form* 27 *August* 1993)

Abstract—A semi-theoretical model is developed to predict liquid-side particulate fouling in enhanced tubes. The model predicts fouling behavior for a wide range of particle size distribution and foulant concentration. In this study, the deposition model uses a coefficient, K_D, which includes two effects, (a) Brownian diffusion in the sticking (or wall) region and (b) momentum transfer to the sticking region. The sticking probability and bond strength factor are defined by empirical correlations as a function of particle size, concentration, and shear stress. The fouling data used in the correlations were taken for concentrations between 2000 and 800 p.p.m. for the particle sizes of 2, 4 and 16 μm. The average fluid velocity in the tube was varied between 1.22 and 2.44 m s^{-1}. The theoretical predictions are in general in good agreement with the experimental data.

INTRODUCTION

FOULING of heat transfer equipment is defined as the deposition of unwanted material on heat exchange surfaces. The deposit causes degradation in thermal and hydraulic performance of the equipment. A combination of two or more fouling mechanisms may occur simultaneously. However, it is important to study each mode separately for better understanding of the individual mechanisms. Particulate fouling is investigated in this paper.

The first significant attempt to derive a general fouling model was by Kern and Seaton [1] who observed from particulate fouling data that the fouling curves usually demonstrate an asymptotic form. Therefore, they postulated that the net fouling rate is expressed as the difference between the deposition and the removal rate. Most investigators use Kern and Seaton's [1] general fouling model as their starting point. However, they differ in their formulation of the deposition and removal rate. Although these models can predict particulate fouling in plain tubes for various flow conditions and concentration, they are limited for a specific deposition region or particle diameter. In addition, experimental results (Webb and Kim [2] and Webb and Chamra [3]) show that the fouling rate is higher for enhanced tubes than for plain tubes. Therefore, the plain tube fouling models underpredict the fouling potential of enhanced tubes.

The removal rate is generally assumed to be proportional to the ratio of the shear stress to the deposit strength factor, and is also proportional to the deposit thickness since particles are more likely to be ablated at larger thickness. However, the deposition rate is different for each fouling model depending on the deposition regimes. Gudmundsson [4] identified three main deposition regimes; diffusion, inertia and impaction. The different regimes are identified according to the size of the suspended particles. In the diffusion regimes, the particles are very small and are carried to the wall by Brownian motion through the viscous sublayer in the case of a turbulent flow. In the inertia regime, the particles are sufficiently large that turbulent eddies give the particles a radial velocity not completely dissipated in the boundary layer. In the impaction regime, the particles are very large and the particle velocity towards the wall approaches the friction velocity.

Kim and Webb [5] developed the first model to predict the fouling behavior of repeated rib tubes. However, the deposition model was limited to the diffusion regime or to very small particles (in the order of 0.3 μm). For larger particle sizes, Kim and Webb's [5] model would underpredict the deposition coefficient since the model does not take into consideration the inertia of the larger particle sizes. In this study, the deposition rate will be modeled to cover a wide range of particle size distribution. This model is the first attempt to predict deposition onto rough surfaces covering both diffusion and inertia regimes.

The experimental data used in this study are reported by Chamra and Webb [6]. They investigated particulate fouling in enhanced and plain tubes. The Wieland NW, Wolverine Korodense, and a plain tube were chosen for testing. The tested tubes are shown in Fig. 1. Fouling data were taken for a wide range of particle concentrations, particle size, and velocity. The concentration was varied between 800 and 2000 p.p.m. for the particle sizes of 2, 4 and 16 μm. In addition, the Reynolds number was varied between 24 000 and 65 000 for a constant concentration of 1500 p.p.m. Chamra and Webb's [6] experimental results showed that the enhanced tubes foul faster than the plain tube. However, at very low concentration the

NOMENCLATURE

A	surface area between ribs [m^2]
B	constant in equation (4)
C_1	constant in equation (3)
C	particle concentration [p.p.m.]
C_d	drag coefficient [dimensionless]
D	Brownian diffusivity [m^2 s^{-1}]
D_i	tube-side diameter [m]
d_p	particle diameter [μm]
dR_f/dt	net fouling rate [m^2 K J^{-1}]
e	surface roughness height [mm]
e^+	dimensionless surface roughness, eu^*/v
f	fanning friction factor [dimensionless]
g	displacement of the velocity profile [mm]
g^+	dimensionless displacement of the velocity profile, gu^*/v
k_f	thermal conductivity of the deposit [W m^{-1} K^{-1}]
K_B	Boltzmann constant, 1.38 E$-$23 J K^{-1}
K_D	particle deposition coefficient defined by equation (11) [m s^{-1}]
K_m	particle transfer coefficient defined by equation (14) [m s^{-1}]
m	mass of particle [kg]
m_f	foulant mass rate [kg s^{-1}]
N	particle mass flux, m_f/A [kg m^{-2} s^{-1}]
n	constant in equation (14)
p	pitch of the rib [mm]
P	sticking probability [dimensionless]
Pr	Prandtl number, v/α [dimensionless]
R	tube radius [mm]
R_p	particle radius [μm]
Re	Reynolds number, $D_i u_m/v$ [dimensionless]
R_f	fouling resistance [m^2 K W^{-1}]
R_f^*	asymptotic fouling resistance [m^2 K W^{-1}]
S	particle stopping distance [mm]
S^+	dimensionless particle stopping distance, Su^*/v
Sc	Schmidt number, v/D [dimensionless]
St	heat transfer Stanton number, $h_i/\rho\, u_m c_p$ [dimensionless]
St_m	mass transfer Stanton number, K_m/u_m [dimensionless]
t	time [s]
T	absolute temperature [K]
t_r	particle relaxation distance [m]
t_r^+	dimensionless particle relaxation distance
u	velocity at distance y [m s^{-1}]
u_o	particle initial velocity toward the surface [m s^{-1}]
u_m	average fluid velocity [m s^{-1}]
u_e^+	friction roughness function defined by equation (20) [dimensionless]
V_B	Brownian velocity [m s^{-1}]
V_{fl}	fluid velocity normal to the surface [m s^{-1}]
V_{fl}^+	dimensionless fluid velocity, V_{fl}/u^*
V_r	radial fluctuating velocity of particle [m s^{-1}]
x_f	thickness of the deposit [mm].

Greek symbols

ξ	deposit strength factor [N s m^{-2}]
ρ	density [kg m^{-3}]
τ_s	surface shear stress [N m^{-2}]
ϕ_d	rate of deposition [kg m^{-2} s^{-1}]
ϕ_r	rate of removal [kg m^{-2} s^{-1}].

Subscripts

b	bulk
f	foulant
fl	fluid
KD	Korodense tube
NW	NW tube
p	particle
R	rough surface
ref	reference
s	surface
sm	smooth surface.

enhanced and plain tubes foul at the same rate. The asymptotic fouling resistance increases as the concentration increases and it decreases as the particle diameter and velocity increase.

FOULING MODEL

According to Kern and Seaton [1], the net fouling rate is expressed as the difference between the deposition rate and removal rate,

$$\rho_f k_f \frac{dR_f}{dt} = \phi_d - \phi_r. \quad (1)$$

The deposition rate is expressed as,

$$\phi_d = K_D C_b \quad (2)$$

and the removal rate is expressed as,

$$\phi_r = C_1 \frac{\tau_s}{\xi} x_f. \quad (3)$$

Combining equations (1), (2) and (3) and taking $x_f = R_f k_f$, results in a differential equation that can be solved to yield

$$R_f = R_f^*(1 - e^{-Bt}) \quad (4)$$

where

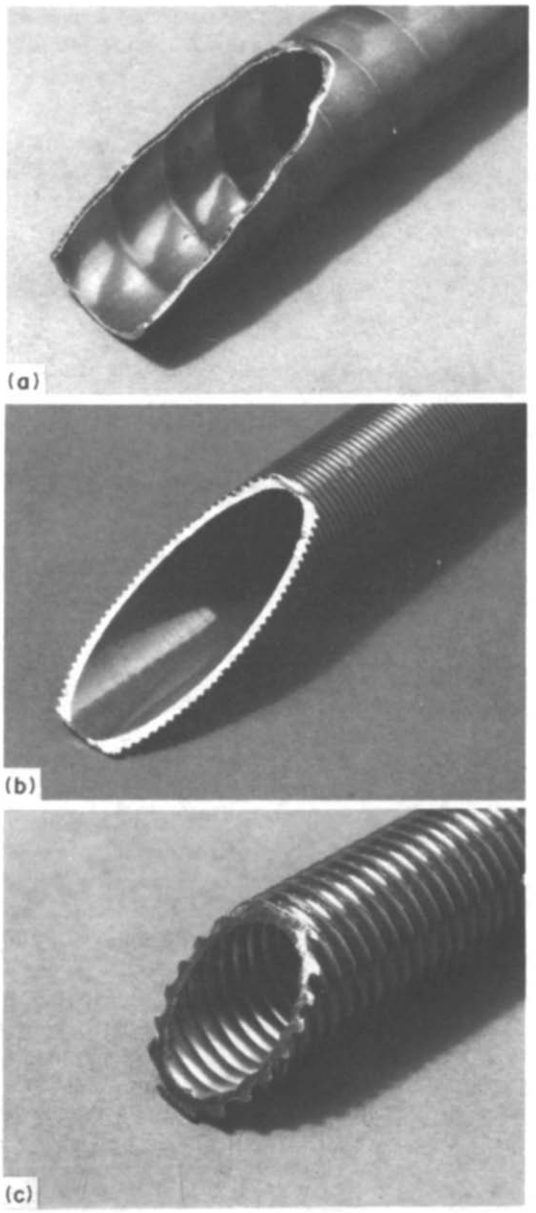

FIG. 1. (a) Korodense, (b) plain, and (c) NW tube geometries.

$$R_f^* = \frac{K_D C_b \xi}{C_1 \tau_s k_f} \tag{5}$$

$$B = \frac{C_1 \tau_s}{\xi \rho_f}. \tag{6}$$

The above equations can be used to predict fouling behavior of enhanced tubes provided that K_D, τ_s, ξ, k_f, ρ_f and C_1 are known.

FORMULATION OF THE DEPOSITION COEFFICIENT, K_D

The development of the deposition coefficient, K_D, should cover both the diffusion and inertia regimes. This is because the actual fouling process involves a wide range of particle sizes.

The particle flux in the wall region may be expressed as

$$N_s = K_m(C_b - C_s). \tag{7}$$

If some particles do not quite reach the wall and if some do not stick on impact, Beal [7] postulated that there will be an accumulation in the boundary layer near the wall, and C_s will increase from an initial value of zero to a steady-state value. This non-zero concentration will inhibit the transport of particles so that only enough particles are transported to the wall to replace those which deposit on the surface. The flux of particles depositing on the wall from the region within the particle stopping distance, S^+ can be written as

$$N = V_r P C_s \tag{8}$$

where V_r is the radial velocity of particles from both fluid motion and Brownian motion. The stopping distance (S) is defined as the distance travelled by a particle in a free flight when it acquired an initial velocity, u_o. The initial velocity is assumed to be equal to the radial velocity fluctuation V_r. From this definition the stopping distance is related to the particle relaxation time (t_r) as

$$S = V_r t_r. \tag{9}$$

Now, we assume that the mass flux of particles into the region within S^+ is equal to the mass flux of particles to the wall ($N = N_s$). This assumption is predicated on C_s being a steady-state concentration. This condition is reached quickly so that the period during which C_s is building up to its steady-state value can be neglected. With these assumptions, we can solve equations (7) and (8) simultaneously to give

$$\frac{N}{C_b} = \frac{K_m P V_r}{K_m + P V_r}. \tag{10}$$

From the above equation, the deposition coefficient, K_D, is expressed as

$$K_D = \frac{K_m P V_r}{K_m + P V_r}. \tag{11}$$

All the parameters in equation (11) will be modeled in the next sections.

FORMULATION OF THE MASS TRANSPORT COEFFICIENT, K_m

The mass transport coefficient (K_m) was formulated by applying the heat and mass transfer analogy. The heat transfer correlation used for the analogy is given by Webb *et al.* [8]. This correlation was based on the application of a heat-momentum transfer analogy to flow over a rough surface having repeated-rib roughness. The rough surface Stanton number is

$$St_R = \frac{f_R/2}{1+\sqrt{(f_R/2)}(g(e^+)\,Pr^n - u_c^+(e^+, p/e))}. \quad (12)$$

Webb *et al.* [8] correlated the heat transfer data for a wide range of repeated rib roughness by

$$g(e^+) = 4.75(e^+)^{0.28}. \quad (13)$$

The Prandtl number function was found to be $F(Pr) = Pr^{-0.57}$ for a wide range of e^+ ($20 < e^+ < 1000$). Later, Webb *et al.* [8] found that the same correlation can be used to predict the performance of the repeated rib tubes with different rib cross section (circle, semi-circle, etc.).

For rough surfaces, equation (12) may be used to obtain the mass transport coefficient by substituting Pr for Sc, and St for the mass transfer Stanton number, St_m.

$$St_m = \frac{K_m}{u_m} = \frac{f_R/2}{1+\sqrt{(f_R/2)}(g(e^+)\,Sc^n - u_c^+)}. \quad (14)$$

The Sc exponent for repeated roughness was found to vary between 0.5 and 0.58. The 0.5 exponent was verified by Davies [9] for small aerosol particles. This dependency should be tested for particles suspended in liquids. Dawson and Trass [10] correlated their mass transfer data, taken for six similar surfaces with V-shaped grooves roughness, to obtain an exponent of 0.58 for Sc between 390 and 4600. Their Sc exponent agrees closely with the 0.57 value of Webb *et al.* [8]. Thus, the value of 0.57 appears to be applicable to wide range of roughness geometries and covers a wide Schmidt number range. This value was confirmed by Chamra and Webb [6]. They correlated particulate fouling data and showed that the asymptotic fouling resistance is proportional to $Sc^{-0.57}$ for different enhanced tubes.

The Schmidt number of the suspended particles is of the order of 10^5–10^6. Therefore, for high Sc numbers ($=10^5$ 10^6) equation (17) becomes

$$St_m = \frac{K_m}{u_m} = \frac{\sqrt{(f_R/2)}}{g(e^+)\,Sc^{0.57}}. \quad (15)$$

Webb *et al.* [8] found the following form of $g(e^+)$ function for the repeated rib tubes with $0.01 \leqslant e/D \leqslant 0.04$ and $10 \leqslant p/e \leqslant 40$.

$$g(e^+) = 8.5(e^+)^{0.1} \quad \text{for} \quad 10 < e^+ < 20 \quad (16)$$

$$g(e^+) = 4.75(e^+)^{0.28} \quad \text{for} \quad e^+ > 26. \quad (17)$$

For this study, the tested tubes have geometry with $0.014 \leqslant e/D \leqslant 0.025$ and $9 \leqslant p/e \leqslant 20$, where e^+ is between 26 and 99.

DETERMINATION OF THE RADIAL VELOCITY OF PARTICLES, V_r

The radial velocity of particles is needed to evaluate the deposition coefficient K_D (equation (11)). The radial velocity of particles close to the wall is considered to consist of two components, one part due to a fluid motion normal to the wall, V_{fl}, and the other part due to Brownian motion of the particle itself, V_B,

$$V_r = V_{fl} + V_B. \quad (18)$$

The Brownian motion velocity can be determined by considering that it is caused by molecules of the fluid striking the particles. According to Jeans [11], the Brownian velocity for smooth tubes is given by,

$$V_B = \left(\frac{K_B T}{2\pi m}\right)^{1/2}. \quad (19)$$

The Brownian motion velocity is independent of the surface geometry, therefore equation (19) is applicable to rough surfaces. The particle velocity due to fluid motion is determined from Davies' [12] velocity correlation. Davies [12] used the experimental data of Laufer [13] in his correlation. The velocity for a smooth wall is represented by:

$$V_{fl}^+ = \frac{y^+}{y^+ + 10}. \quad (20)$$

The relation given by equation (20) can be used to evaluate V_{fl} once the distance y from the surface is known. In the case of a rough surface, the distance y was taken as the distance from the particle's center, at the moment of starting the free flight, to the shifted origin of velocity profile for given flow conditions. The shift in the velocity profile is due to the roughnesses. For a rough surface, it was observed that the boundary layer behaves as if its origin is located some distance below the crests of the roughness elements. This means that the effect of the surface roughness on the velocity profile outside the sub-layer is to shift the origin to some point below the crests of the roughness. Thus, y^+ was replaced by the rough surface stopping distance, S_R^+, then

$$V_{fl}^+ = \frac{S_R^+}{S_R^+ + 10}. \quad (21)$$

The dimensionless rough surface stopping distance S_R^+ is given by

$$S_R^+ = V_r^+ t_r^+ \quad (22)$$

where t_r^+ is the dimensionless particle relaxation time, given by

$$t_r^+ = \frac{\rho_p d_p^2 u^{*2}}{18\mu\nu}. \quad (23)$$

The particle stopping distance for enhanced tubes is calculated using Browne's [14] particle capture distance concept. However, the standard deviation of the roughness height is set to be equal to zero since the enhanced tubes have uniform roughness height. Assuming that contact with any roughness element results in particle capture, the stopping distance is taken as

$$S_R = S + R_p + e - g. \quad (24)$$

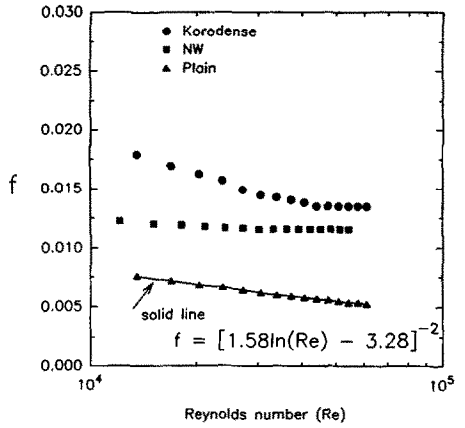

FIG. 2. Friction factors vs Reynolds number.

The displacement of the velocity profile, g, is found by using the correlation obtained by Grass [15] where

$$g^+ = 0.53e^+ + 0.0034e^{+2}. \quad (25)$$

Grass [15] used sand grain roughnesses to obtain his experimental data. A similar equation may be found for different enhancement; however, a detailed measurement of turbulent velocity close to roughness boundaries is needed. As an approximation, equation (25) was used to determine the velocity displacement of the enhanced tubes used in this study.

FRICTION TEST

The friction factors for the tested tubes were measured using the fouling apparatus described by Chamra and Webb [6]. The friction factors were based on the pressure drop over a 3048 mm test section length. The enhanced and plain tube friction factors are shown in Fig. 2. The plain tube friction data were compared with the Filonenko's [16] equation which show good agreement. The Filonenko equation is written as

$$f = (1.58 \ln (Re) - 3.28)^{-2}. \quad (26)$$

The rough friction factors attained a 'fully rough' condition, for which the friction factor is independent of Reynolds number.

Figure 3(a) shows the predicted mass transport coefficient, K_m, for the three tubes (NW, Korodense, and plain tubes) plotted as a function of Reynolds number. As expected, the transport coefficients of the enhanced tubes are larger than that of the plain tube. The higher than expected enhanced tubes' transport coefficient is the result of operating in both diffusion and inertia regions. In addition, the transport coefficient of the NW tube is larger than that of the Korodense tube.

DETERMINATION OF THE WALL SHEAR STRESS, τ_s

The wall shear stress was determined using the model developed by Kim and Webb [5]. Based on the

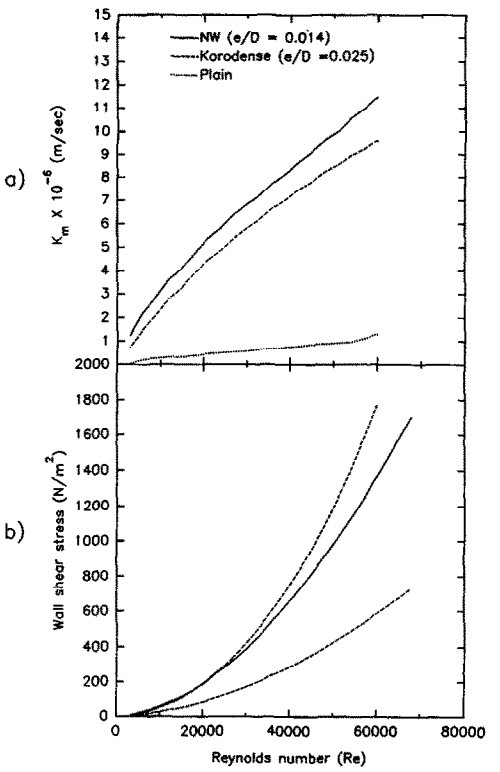

FIG. 3. Transport coefficient K_m and wall shear stress vs Reynolds number.

flow structure between ribs, a four region model given by equation (27) was developed.

$$A_s\tau_s = A_1\tau_1 + A_2\tau_2 + A_3\tau_3 + A_4\tau_4. \quad (27)$$

Region 1 is a forward flow region on top of the rib, region 2 is a recirculating region behind the rib, region 4 is a recirculating region in front of the rib, and region 3 is a forward flow region between regions 2 and 4.

The Lewis [17] model was developed for tubes having rectangular rib cross-sections. In this study, the roughness has a circular shape for the enhanced tubes. In a later paper, Lewis [18] extended his model to other shapes, including three dimensional and circular elements, by means of form drag coefficients for these elements and by invoking the concept of 'equivalent rectangular rib geometry'. The drag coefficient, C_d, will vary with the surface geometry. For the NW and Korodense tubes the rib cross section is circular; therefore the drag coefficient, C_d, is equal to 0.8 for this particular geometry.

Figure 3(b) shows the predicted wall shear stress against Reynolds number. The figure shows that the higher e/D of the Korodense tube results in higher wall shear stress than for the NW tube.

CURVE-FIT OF THE EXPERIMENTAL DATA

The fouling data of Chamra and Webb [6] showed asymptotic behavior, and were curve-fitted into an asymptotic form

Table 1. Asymptotic fouling resistances for enhanced tubes

			Korodense	NW
Re Dimensionless	C_b p.p.m.	d_p μm	R_f^* $m^2 K W^{-1}$	R_f^* $m^2 K W^{-1}$
36000	2000	2	2.78×10^{-5}	3.72×10^{-5}
36000	1500	2	2.29×10^{-5}	3.37×10^{-5}
36000	1200	2	1.99×10^{-5}	2.65×10^{-5}
36000	800	2	1.14×10^{-5}	1.18×10^{-5}
24000	1500	2	3.76×10^{-5}	6.15×10^{-5}
48000	1500	2	0.39×10^{-5}	0.49×10^{-5}
36000	2000	4	1.95×10^{-5}	3.03×10^{-5}
36000	1500	4	0.80×10^{-5}	1.50×10^{-5}
36000	1200	4	0.37×10^{-5}	0.53×10^{-5}
36000	800	4	0.12×10^{-5}	0.32×10^{-5}
24000	1500	4	1.91×10^{-5}	3.80×10^{-5}
48000	1500	4	0.14×10^{-5}	0.21×10^{-5}
36000	2000	16	0.56×10^{-5}	1.07×10^{-5}
36000	1500	16	0.33×10^{-5}	0.90×10^{-5}
36000	1200	16	0.12×10^{-5}	0.16×10^{-5}
24000	1500	16	0.92×10^{-5}	2.64×10^{-5}
48000	1500	16	0.09×10^{-5}	0.12×10^{-5}

$$R_f = R_f^*(1 - e^{-BP}). \tag{28}$$

The curve-fit is needed to reduce R_f^*, B, P, and ξ from experimental data. Table 1 lists the asymptotic fouling resistances for the enhanced tubes. The asymptotic fouling resistance decreases as the Reynolds number increases, the particle diameter increases, and as the concentration decreases. The asymptotic fouling resistance of the Korodense tube is less than that of the NW tube for the same Re, and foulant concentration. This is because the larger e/D and p/e of the Korodense tube results in a higher wall shear stress, resulting in lower asymptotic fouling resistance.

STICKING PROBABILITY, P, AND THE DEPOSIT BOND STRENGTH FACTOR, ξ

The results are presented relative to those of the smooth tube. The reason for this is to avoid the evaluation of the deposit density, ρ_f, and the deposit thermal conductivity, k_f. It is anticipated that the smooth tube particulate fouling values will depend on the Reynolds number even for the same fouling material. Thus, a reference Reynolds number must be specified. In this study, P_{ref}, ξ_{ref} are defined as the values obtained for a smooth tube at the lowest Reynolds number (=24000) and particle diameter (=2 μm), and the highest concentration (=2000 p.p.m.).

The asymptotic fouling resistance and the constant B were obtained from the curve-fitted data. Then, the deposit strength factor ratio was calculated using equation (7) where the constant C_1 is assumed to be equal for smooth and enhanced tubes. The calculated values were used to find the deposition coefficient ratio

$$\frac{K_D}{K_{D,ref}} = \frac{\tau_s}{\tau_{s,ref}} \frac{\xi_{ref}}{\xi} \frac{R_f^*}{R_{f,ref}^*}. \tag{29}$$

Table 2. Sticking probability and deposit bond strength factor for the NW tube

Re	τ_s Pa	C_b p.p.m.	d_p μm	P_{NW}/P_{ref}	ξ_{NW}/ξ_{ref}
36000	502	2000	2	0.70	0.55
36000	502	1500	2	0.60	0.46
36000	502	1200	2	0.53	0.43
36000	502	800	2	0.40	0.38
24000	210	1500	2	0.90	0.62
48000	892	1500	2	0.25	0.30
36000	502	2000	4	0.56	0.58
36000	502	1500	4	0.50	0.53
36000	502	1200	4	0.41	0.51
36000	502	800	4	0.20	0.37
24000	210	1500	4	0.75	0.64
48000	892	1500	4	0.19	0.40
36000	502	2000	16	0.51	0.47
36000	502	1500	16	0.46	0.43
36000	502	1200	16	0.10	0.30
24000	210	1500	16	0.54	0.60
48000	892	1500	16	0.26	0.31

Table 3. Sticking probability and deposit bond strength factor for the Korodense tube

Re Dimensionless	τ_s Pa	C_b p.p.m.	d_p μm	P_{KD}/P_{ref}	ξ_{KD}/ξ_{ref}
36000	578	2000	2	0.62	0.46
36000	578	1500	2	0.54	0.37
36000	578	1200	2	0.46	0.35
36000	578	800	2	0.38	0.33
24000	258	1500	2	0.77	0.58
48000	1085	1500	2	0.22	0.29
36000	578	2000	4	0.45	0.43
36000	578	1500	4	0.43	0.45
36000	578	1200	4	0.37	0.32
36000	578	800	4	0.17	0.29
24000	258	1500	4	0.64	0.54
48000	1085	1500	4	0.17	0.28
36000	578	2000	16	0.44	0.43
36000	578	1500	16	0.32	0.32
36000	578	1200	16	0.07	0.30
24000	258	1500	16	0.47	0.54
48000	1085	1500	16	0.20	0.23

Then, the sticking probability ratio can be approximated from equation (11).

$$\frac{P}{P_{ref}} = \frac{K_{m,ref}}{K_m} \frac{K_D}{K_{D,ref}} \frac{V_{r,ref}}{V_r}. \tag{30}$$

Tables 2 and 3 list the values for P/P_{ref} and ξ/ξ_{ref} for the NW and Korodense tubes, respectively. The P/P_{ref} values shown in Tables 2 and 3 were correlated using a least squares fit program. The surface shear stress τ_s, geometric ratios e/D and p/e, particle diameter, and foulant concentration were chosen as functional groups. The functional groups were chosen based on the work of other investigators. Based on fluid dynamic fundamentals, Watkinson and Epstein [19] showed that the sticking probability is inversely proportional to the shear stress. In addition, Beal [20] showed the sticking probability dependence on fluid velocity (or shear stress) and particle diameter for

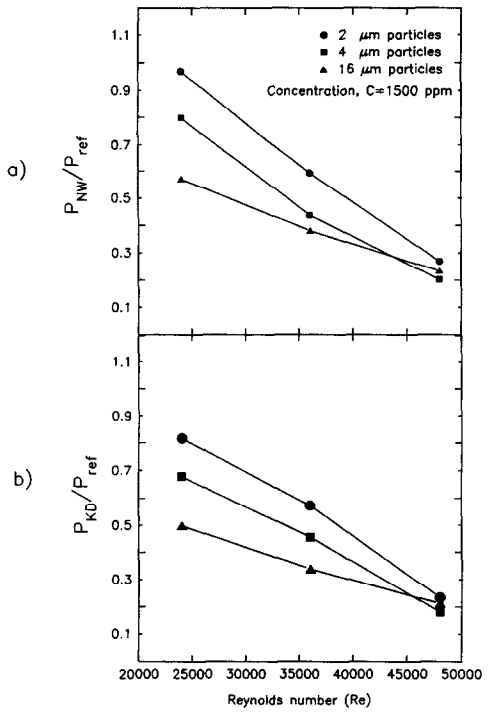

FIG. 4. Sticking probability vs Reynolds number for (a) NW tube, (b) Korodense tube.

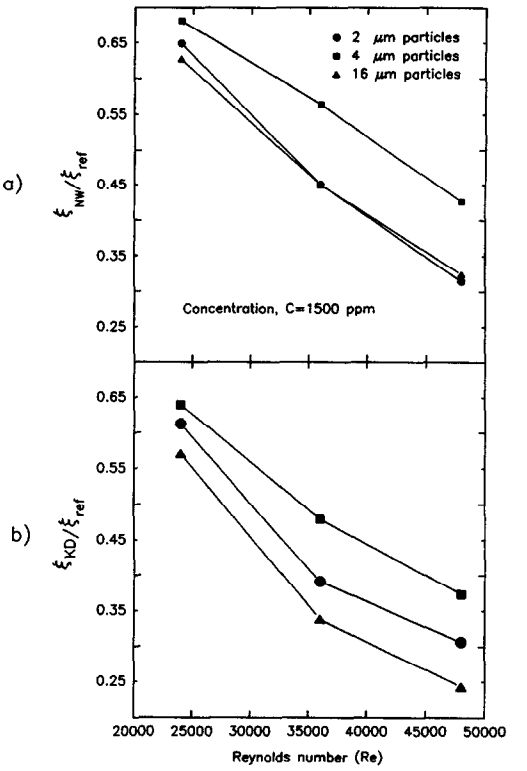

FIG. 5. Deposit bond strength vs Reynolds number for (a) NW tube, (b) Korodense tube.

particles in the inertia regime. The geometric dependency was studied by Kim and Webb [5] who correlated their experimental data to show that the sticking probability ratio is proportional to $(e/D)^{-0.3}$ and $(p/e)^{0.6}$.

The sticking probability ratio was first correlated separately for the NW and Korodense tubes. The correlations are presented in the following equations for the NW and Korodense tubes, respectively.

$$\frac{P_{NW}}{P_{ref}} \propto \tau_s^{-0.67} d_p^{-0.29} C_b^{1.0} \tag{31}$$

$$\frac{P_{KD}}{P_{ref}} \propto \tau_s^{-0.72} d_p^{-0.32} C_b^{1.04}. \tag{32}$$

Equations (31) and (32) show that the sticking probability ratio decreases as τ_s increases. This is because the sticking probability is inversely proportional to the wall shear stress if the hydrodynamic force controls the particle adhesion. The equations also show that the sticking probability ratio decreases as d_p increases. The exponents in the above equations are in approximate agreement for all parameters. This suggests that the chosen functional group are indeed correlating parameters, with negligible dependence on surface geometry. Figure 4 shows the sticking probability ratio vs Reynolds number for the NW and Korodense tubes.

Figure 5 shows the deposit bond strength factor ξ vs Reynolds number for the NW, and Korodense tubes. The figure shows that the deposit bond strength factor decreases as the Reynolds number increases. In addition, the deposit strength factor increases in the diffusion regime as the particle diameter increases. However, it starts decreasing again in the inertia regime. The deposit bond strength factor is correlated using the least square fit. The correlations for the NW and Korodense tubes are

$$\frac{\xi_{NW}}{\xi_{ref}} \propto \tau_s^{-0.37} d_p^{-0.08} C_b^{0.40} \tag{33}$$

$$\frac{\xi_{KD}}{\xi_{ref}} \propto \tau_s^{-0.50} d_p^{-0.07} C_b^{0.44}. \tag{34}$$

Equations (33) and (34) show that the deposit strength factor ratios have weak dependence on the particle diameter. Also, the exponents show approximate agreement for both enhanced tubes as was observed for the sticking probability.

The developed correlations need to be generalized to be used with other enhanced tubes. The small difference in exponents may be due to the different tube geometry used. Therefore, the sticking probability and deposit bond factor ratios were generalized by including the effects of the geometric parameters $(e/D, p/e)$.

$$\frac{P}{P_{ref}} \propto \tau_s^{-0.72} d_p^{-0.32} C_b^{1.02} (e/D)^{-0.30} \tag{35}$$

$$\frac{\xi}{\xi_{ref}} \propto \tau_s^{-0.43} d_p^{-0.07} C_b^{0.42} (e/D)^{-0.4}. \tag{36}$$

Table 4. Comparison of the results with the previous models for enhanced tubes

Model	R_f^*	P	ξ
Kim and Webb [5]	−3.65	−1.97	−0.52
Current results	−3.93	−1.59	−0.66

The geometric variable p/e was dropped from the correlations because it was not sufficiently varied to be taken into account. Even though only two different enhanced tubes were tested in this study, the exponent of e/D is in good agreement with the exponent obtained by Kim and Webb [5] on transverse rib roughness.

COMPARISON WITH PREVIOUS FOULING CORRELATION

The current fouling tests were compared with the fouling results of Kim and Webb [5] who used transverse rib tubes in their tests. Kim and Webb [5] correlated their data as a function of Reynolds number for the plain tube, and added geometric variables in the case of enhanced tubes. Kim and Webb's [5] experimental data were re-correlated using the fouling model developed in this paper. The same functional groups were used in order to compare with the present model. Table 4 compares the Reynolds number exponents of the referenced models with the test results for the enhanced tubes.

Table 4 shows that the current results reasonably match the re-correlation of Kim and Webb's data for transverse rib tubes. The difference between the exponents is because the current results are applicable to both diffusion and inertia regimes.

APPLICATION TO HEAT EXCHANGER DESIGN

The model developed in this study can be directly used to assess the fouling potential of any enhanced tube relative to that of a plain tube. The correlations for sticking probability and deposit strength factors can be used with the fouling model to predict the asymptotic fouling resistance. The asymptotic fouling of the Korodense tube relative to a plain tube can be compared as follows.

From equation (6), the asymptotic fouling resistance is given by

$$R_f^* \propto \frac{K_D \xi C_b}{\tau_s}. \tag{37}$$

The sticking probability and deposit strength factor ratios were substituted in equations (29) and (6). Combining both equations yields

$$\frac{R_{f,KD}^*}{R_{f,sm}^*} = d_p^{0.07} C_b^{-0.4} \frac{\tau_{s,KD}^{-2.23} K_{m,sm} V_{r,KD}}{\tau_{s,sm}^{-2.74} K_{m,KD} V_{r,sm}} \tag{38}$$

where subscripts KD and sm denote the Korodense and plain tube, respectively.

Table 5. Predicted asymptotic resistance ratio for different concentrations and particle diameter at $Re = 36\,000$

Particle diameter, d_p (μm)	Concentration, C_b (p.p.m.)	$R_{f,KD}^*/R_{f,sm}^*$
2	2000	2.870
2	1500	1.640
2	1200	1.800
2	800	2.100
2	600	2.340
2	300	3.060
67% 2 and 33% 4	2000	2.210
50% 2 and 50% 4	2000	2.160
33% 2 and 67% 4	2000	2.040
4	2000	1.940
16	2000	1.750
2	300	3.060

The asymptotic fouling resistance ratio can be evaluated for any flow conditions where the surface shear stress can be found from Fig. 3(b), the particle transfer coefficient can be found from Fig. 3(a), and the radial velocity is evaluated from equation (18). For example, the asymptotic fouling resistance ratio is evaluated for $Re \simeq 36\,000$ corresponding to a velocity of 1.8 m s^{-1}, and for 2 μm particle diameter. All the variables in equation (38) are held constant except the concentration. This will make it possible to predict the asymptotic ratio for a lower concentration than used in this study. The results are shown in Table 5.

Table 5 shows that the asymptotic fouling resistance for the Korodense tube is higher than that for the smooth tube. In addition, the asymptotic fouling resistance ratio increases as the concentration decreases.

Table 5 also shows the predicted asymptotic fouling resistance ratio for different particle size. The concentration and Reynolds number are held constant at 2000 p.p.m. and 36 000, respectively. The Schmidt number for the mixture is calculated by taking the weighted average of the particle diameter. Table 5 shows the asymptotic fouling resistance ratio decreases as the particle diameter increases.

CONCLUSIONS

A semi-empirical fouling model was developed to predict particulate fouling in enhanced tubes. The deposition model was developed to take into account the presence of particle size distribution in the foulant. The fouling model can predict the asymptotic fouling resistance for enhanced tubes with different concentration, velocity, and particle size. The fouling resistances are predicted relative to a plain tube operating at a reference condition.

The sticking probability and the deposit bond strength factor were correlated as function of the surface shear stress, particle diameter, and the concentration. The correlations for the enhanced and plain tubes are given in equations (31)–(34). The above correlations show that the chosen functional

groups indeed correlate the sticking probability and deposit strength factor since the exponents of all the equations are in good agreement.

The fouling model was used to compare the asymptotic fouling resistances of two enhanced tubes and a plain tube. The asymptotic fouling resistances of the enhanced tubes were found to be higher than those of the plain tube. In addition, the asymptotic fouling resistance increases as the concentration increases and the particle diameter and the surface shear stress decrease.

REFERENCES

1. D. Q. Kern and R. A. Seaton, A theoretical analysis of thermal surface fouling, *Br. Chem. Engng* **4,** 258–262 (1959).
2. R. L. Webb and N.-H. Kim, Particulate fouling of internally-ribbed tubes. In *Heat Transfer Equipment Fundamentals, Design, Applications and Operating Problems* (Edited by R. K. Shah), Vol. HTD-108, pp. 315–324 (1989).
3. R. L. Webb and L. M. Chamra, On-line cleaning of particulate fouling in enhanced tubes. In *Fouling and Enhancement Interactions* (Edited by T. J. Rabas and J. M. Chenoweth), Vol. ASME HTD-164, pp. 47–54 (1991).
4. J. S. Gudmundsson, Particulate fouling. In *Fouling of Heat Transfer Equipment* (Edited by E. F. C. Somerscales and J. G. Knudsen), pp. 357–387. Hemisphere, Washington, D.C. (1981).
5. N.-H. Kim and R. L. Webb, Particulate fouling of water in tubes having a two-dimensional roughness geometry, *Int. J. Heat Mass Transfer* **30,** 2727–2738 (1990).
6. L. M. Chamra and R. L Webb, Effect of particle size distribution on particulate fouling in enhanced tubes, *J. Enhanced Heat Transfer* **1**(1), 65–75 (1993).
7. S. K. Beal, Deposition of particles in turbulent flow on channel or pipe walls, *Nucl. Sci. Engng* **40,** 1–11 (1970).
8. R. L. Webb, E. R. G. Eckert and R. J. Goldstein, Generalized heat transfer and friction correlations for tubes with repeated-rib roughness, *Int. J. Heat Mass Transfer* **15,** 180–184 (1971).
9. J. T. Davies, *Turbulence Phenomena.* Academic Press, New York (1972).
10. D. A. Dawson and O. Trass, Mass transfer at rough surfaces, *Int. J. Heat Mass Transfer* **15,** 1317–1336 (1972).
11. J. Jeans, *An Introduction to the Kinetic Theory of Gases,* pp. 58–59. Cambridge University Press, New York (1940).
12. C. N. Davies, Deposition of aerosols from turbulent flow through pipes, *Proc. R. Soc. A* **289,** 235–246 (1966).
13. J. Laufer, Structure of turbulence in fully developed pipe flow. N.A.C.A. Rep. 1174 (1954).
14. L. W. B. Browne, Deposition of particles on rough surfaces during turbulent gas-flow in a pipe, *Atmospheric Environment* **8,** 801–816 (1974).
15. A. J. Grass, Structural features of turbulent flow over smooth and rough boundaries, *J. Fluid Mech.* **50,** 233–255 (1971).
16. G. K. Filonenko, Hydraulic research in pipes, *Teploenegetika* **1**(4), 40–44 (1954).
17. M. J. Lewis, An elementary analysis for predicting the momentum and heat transfer characteristics of a hydraulically rough surface, *ASME J. Heat Transfer* **97**(2), 249–254 (1975).
18. M. J. Lewis, Optimising the thermohydraulic performance of rough surfaces, *Int. J. Heat Mass Transfer* **18,** 1243–1248 (1975).
19. A. P. Watkinson and N. Epstein, Particulate fouling of sensible heat exchangers, *4th Int. Heat Transfer Conf.,* Versailles, Vol. 1, Paper HE 1.6 (1970).
20. S. K. Beal, Correlations for the sticking probability and erosion of particles, *J. Aerosol Sci.* **9,** 455–461 (1978).